Utrecht University

Master's Thesis in Nanomaterials Science

Composition and activity of CuAu/Pt core/shell electrocatalytic nanoalloys using first-principles calculations and machine learning

R. van der Kruit BSc

Daily Supervisor: Asst. Prof. Dr. N. Artrith

First Examiner: Asst. Prof. Dr. N. Artrith

Second Examiner: Prof. Dr. F.M.F. de Groot

Debye Institute for Nanomaterials Science

Materials Chemistry and Catalysis

Utrecht, 29 March 2023

Utrecht University

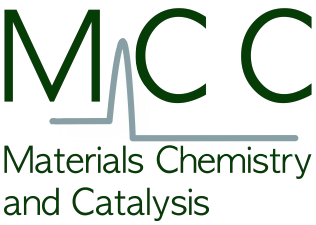

Layperson's Abstract

A metal nanoparticle is a combination of one or more metals that is a few nanometers (10^{-9} meters) in size. A well-known material consisting of multiple metals is brass, which contains copper and zinc, but other metal combinations like gold and platinum are also possible. These particles form an integral part of the modern chemical industry where they are used as *catalysts*. Most modern products have at least one production step involving these particles and recent research indicates that they can be used to make fuels and other useful chemicals from common renewable resources. In general, catalysts are compounds that improve a chemical reaction, such as making hydrogen and oxygen from water, while not being consumed by the reaction. Metal nanoparticles have the advantage that they can be customized to suit their environment and goals by producing them with multiple metals, possibly improving their productivity or bringing down their cost. Computer simulations can be used to screen possible new materials or help understand how or why certain particles work, which is valuable information to help improve existing processes.

This thesis investigated the make-up and structure of a nanoparticle consisting of three metals, namely gold, copper and platinum. Platinum is a very good, but expensive, catalyst. It was expected that adding a layer of platinum on top of gold and copper results in an equally good or better catalyst that is less expensive. This was tested using a theoretical model where the platinum was added on top of the gold and copper surface, and some basic reactions were tested afterwards. The tested reactions were the splitting of oxygen and hydrogen, which are important steps in the formation of water from these gasses in fuel cells. It was found that the investigated surface performed well for these reactions, but only one surface was tested while a particle generally exhibits several different, so more calculations on other surfaces and experimental results are needed.

Abstract

Noble metal nanoparticles continue to be of great interest to the catalysis community for their characteristics, and extensive research has been conducted into bimetallic nanoparticles involving these metals. Inclusion of another metal to form trimetallic particles could further enhance the characteristics of these particles by increasing the possible metal compositions and the associated interactions within a particle. With the increase in possible metal combinations and compositions, theoretical methods can provide assistance in understanding reaction mechanisms or pre-screen metal combinations for their catalytic activity. Machine learning methods can additionally reduce the computational cost of such calculations, but the lack of extensive databases for trimetallic particles hampers their application, requiring the calculation of accurate databases using first-principles methods.

In this work, the composition and formation of a trimetallic CuAu/Pt surface, the adsorption of O, H, C and CO on this surface, and the dissociation of O_2 and H_2 was investigated using density-functional theory and the nudged elastic band method. The Pt-coated CuAu surface was found to form at least one monolayer of Pt in various configurations, ranging from highly ordered to disordered with similar stability. The adsorption of CO and O_2 was found to occur on the top and bridge sites, respectively, whilst H_2 was found to adsorb dissociatively with no discernible energy barrier. The dissociation of oxygen on the surface resulted in molecular oxygen adsorbing on the bridge site and dissociating to atomic oxygen in the hollow site with an energy barrier of 0.22 eV.

Contents

1. Introduction

Catalytic nanoparticles involving noble metals are of great interest to a wide variety of chemical processes with their capability of improved activity and stability making them highly sought after. Examples include the transformation of oxygen or carbon dioxide into high interest products such as carbon-based fuels or syngas via thermo- or electrocatalytic conversion [1–3], and a variety of other oxidation and hydrogenation reactions [4]. The catalytic activity, selectivity for the desired reaction and stability are the main properties of interest when investigating catalysts or designing new catalyst [5]. Monometallic catalysts have long formed the backbone of chemical catalysis, with multimetallic particles forming an increasingly sizeable part of the field.

These multimetallic particles have been of great interest for a long time due to their capability of improving the catalyst characteristics compared to their monometallic counterparts [6], with the bulk of the progress being performed using bimetallic particles. The structure and composition of these multimetallic particles was found to depend on the concentrations of the component materials and the energies of the inter-species bonds compared to the bulk materials [7]. Furthermore, the various metals in these particles can have synergistic effects between the component metals, improving the selectivity, activity and/or stability of the nanoparticle[8]. A variety of factors contribute to these synergistic effects, such as the strain around the active site [9, 10], particle size or synthesis conditions [4, 11]. For example, the strain in a metal surface can promote the overlap between the electron orbitals and influence the electronic properties of the surface [12]. This change in electronic properties can manifest itself as a lowering of the d-band energy when a monolayer of a 2nd metal is added on a bulk material [9].

Recently, there has been an increased interest in trimetallic systems and their potential to further enhance the metal nanoparticle (NP) characteristics. However, the addition of a third element vastly increases the available design space for NP's due to an increase in possible metal combinations and ratios. This wider possible scope lends itself well to preliminary or supporting research using density functional theory (DFT) and/or machine learning [13], since this would partially alleviate the time and resource intensive synthesis for a wide variety of possible combinations. An example can be found in Pt-based NP's, where the research in monometallic particles [14] has been heavily augmented by research into the combination of this precious metal with base metals into bimetallic particles [8, 15] with limited research on the trimetallic combinations possible [16].

1.1. Aims of the Project

The aim of this project is to investigate the composition, structure and catalytic properties of trimetallic CuAu/Pt nanoparticles using theoretical methods, with the scope being limited to the (100) surface. The project has been split into two sections; First, the composition of a Pt-coated CuAu surface was explored on a Au-terminated (100) CuAu surface. The goal is to identify possible surface structures and to prepare a surface that will be used for the second part of the thesis. In the second part the adsorption of oxygen, hydrogen and carbon monoxide, and the dissociation of oxygen and hydrogen is investigated. The adsorption and dissociation energies of these species on the theoretical surface serve as an indicator for their performance in more

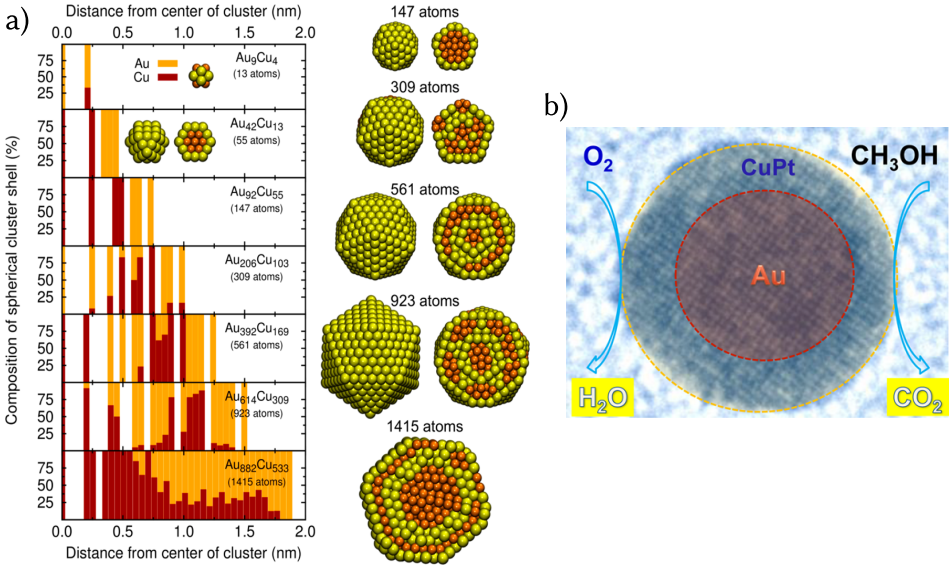

Figure 1: (a) Determined composition of bimetallic CuAu NP's with the cross-section shown using density functional theory and machine learning. (b) The experimental structure of a Au/CuPt core/shell nanoparticle active for methanol oxidation reaction. Reprinted with permission from [11] and [16]. Copyright 2014 American Chemical Society.

realistic environments [9].

1.2. Multimetallic CuAuPt NP structure

For this thesis, a trimetallic CuAu particle with a Pt shell was chosen for its widespread use and interest for the system within the research group. In addition to this, there are prior results for the CuAu core [11, 17] and various bimetallic combinations of Pt with either copper or gold. For the CuAu particles it was found that after heating in a vacuum the particle would be mainly Au-coated with a primarily Cu core of the particle (Figure 1a). In an aqueous environment, on the other hand, the situation was reversed with copper being located mainly on the metal-water interface. Additionally, it has been shown that growing Pt layers on Au results in a Au/Pt core/shell structure [18] and that the distance between the layers contracts slightly [19]. Furthermore, it was found that the Pt atoms will be embedded within a gold shell after heating if the Au-to-Pt ratio is close to 1:1 [20, 21]. The combination of Pt with Cu was also found to form stable a Cu/Pt core/shell structures with enhanced electrochemical activity [22]. When layer growth is undesired, it was shown that the synthesis of alloyed AuPt particles is also possible, and that they can be effective catalysts for the methanol oxidation reaction (MOR) [23]. The structure that is formed when combining metals is generally also an interplay between the bulk characteristics of the component metals and how these interact in the created environment during synthesis [7].

For the trimetallic combinations of Cu, Au and Pt it was shown with theoretical investigations into 147 atom NP's with different Cu, Au and Pt ratios that the the Au or Pt atoms are located

on the outside with Cu generally residing within the structure unless it is present in excess [24]. This segregation of Au towards the outside of the particle was also observed for multiple Au metal combinations in a vacuum, and is attributed to the lower surface energy of Au compared to metals like Cu and Pt. If the particles are placed on a support or in a different environment the effect of this change in environment can result in a different particle morphology [25]. Experimental particles have been synthesized as core/shell particles in aqueous environments resulting in Au/CuPt (Figure 1b)[16] and AuCu/Pt [26] NP's. Both mentioned trimetallic particles were found to be active for the oxygen reduction reaction (ORR).

1.3. O_2 and H_2 Dissociation on Au and Pt Surfaces

With this segregation of Pt and Au towards a shell in mind it is of interest to also investigate what is known regarding the oxygen and hydrogen adsorption and dissociation on Cu, Au and Pt terminated surfaces. A pure Pt system can be taken as a baseline due to their ubiquitous use in the catalysis field. With theoretical methods it was found that the edge sites in clusters is most active, with the bridge and hollow (both fcc and hcp) sites being favourable for O_2 binding on (111) Pt [27], while the (100) Pt surface prefers binding of oxygen on the bridge site [28]. The dissociated molecule was found to favour binding on the fcc hollow site for (111) Pt with it being proposed that oxygen dissociates on the bridge site, followed by migration of the oxygen atoms via the top site towards the hollow [29]. The Au surfaces are relatively inert for oxygen dissociation due to the desorption energy being lower than the activation barrier on pure Au, this can however be improved by selective doping of more reactive metals [28].

For bimetallic CuAu, which forms the core of our target particle, the adsorption of oxygen is stronger on the Cu terminus, compared to Au, which correlates with the tendency for Cu to oxidize [11] and monometallic Au to be active for the reaction [28]. This stronger oxygen adsorption was also calculated for (100) Au/M (M=Cu,Pt) structures, with both the Cu and Pt-coated surfaces having favourable adsorption energies at all oxygen coverages between 0 and 1 monolayer [19]. This stronger adsorption could be explained using DOS calculations for the pure Au and Au/Pt surfaces where the addition of oxygen on the surface resulted in a stronger change in the DOS for the Pt- and Cu-coated surface with the bonding interactions of these surfaces with oxygen being much lower in energy to the Fermi level [19, 30]. When Cu is underneath the Pt outer layer it was found that the adsorption of other intermediates in the ORR is weaker compared to pure Cu [22], indicating that the subsurface layer can have a significant influence on the characteristics of the Pt outer layer.

The application of the trimetallic metal combinations of Cu, Au and Pt for oxygen dissociation has been subject of only a few studies, with two publications finding the Au atoms in the core of the core-shell particle [16, 26]. Both publications highlight experimental results in the synthesis and activity of their trimetallic particle, but lack a mechanistic explanations on why this enhancement is observed. The first particle consisted of a CuPt shell, and it was found that this Au/CuPt NP was more active for oxygen reduction (ORR) and methanol oxidation (MOR) due to the Au core stabilizing the CuPt shell [16]. The other experimental particle was CuAu/Pt, which is also the particle of interest in this thesis, and it was found that it has improved ORR activity due to slight compressive strain created by the CuAu core on the Pt shell [26].

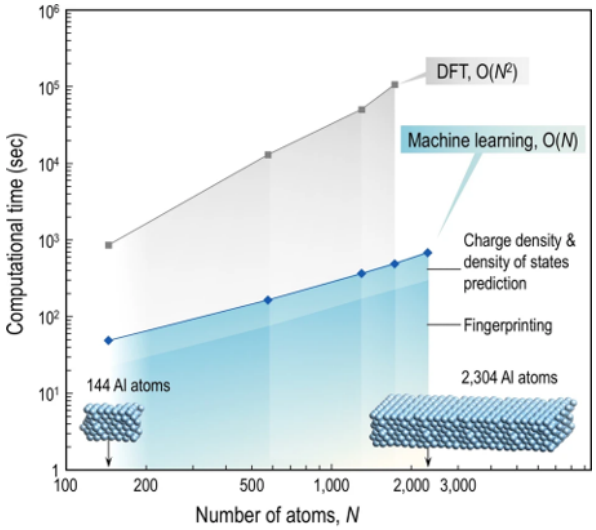

Figure 2: Difference in computation time with system size scaling between machine learning and density functional theory for electronic structure predictions. Adapted with permission from [43].

2. Methods

Using theoretical methods it is possible to dive deeper into the formation of these trimetallic particles and how certain reactions are influenced by the 3 metals compared to 2 or 1 in bi- and monometallic particles. The theoretical, or computational, approaches have long been focussed around first-principles methods like density functional theory (DFT) and machine acceleration of DFT with an increasing use of machine learning models [13].

2.0.1. Density Functional Theory

DFT methods allow for the computational prediction of material properties by approximately solving the Schrodinger equation [31]. In practice, most DFT approaches utilize the Kohn-Sham (KS) equations [32], where a multi-electron system can be approached as a system of multiple non-interacting one electron systems. If the calculation is performed self-consistently, it includes both the electron-ion and electron-electron interactions and can reproduce the correct electron density of the system [33]. KS DFT relies on approximations to the exchange-correlation (XC) energy, and the choice of XC functional is one of the parameters that depends on the goals of the research [34, 35]. The most fundamental approximation is the local density approximation (LDA) [32] which can be improved by taking into account the density gradient and possibly additional constraints to give (meta-) generalized gradient approximation (GGA) methods such as PBE [36] and (r^2)SCAN [37, 38]. Additionally, there are multiple possible approaches used to perform KS calculations. Possible implementations include those based on a projector-augmented-wave (PAW) method [39], as utilized in VASP [40] or Quantum ESPRESSO [41], or on numeric atom-centered orbitals (NAO), as utilized in FHI-AIMS [42].

2.0.2. Machine Learning

Recently, an increasing interest has been displayed in the usage of machine accelerated methods and artificial neural networks for calculations on catalyst materials [11, 44]. This interest is rooted in the high computational cost of DFT calculations once the system size increases [43, 45] (Figure 2), and made possible by advances in computational hardware [33] and the availability of DFT data from open science efforts such as the Materials Project [46]. In essence machine learning models can be seen as constructed models that improve their results in some task, such as determining the energy of structures, trough experience or training [47]. When setting up a machine learning model, how the model learns and what its learning functions or parameters are is of great importance and depends on the application and the types of data used. A broad division can be made by the number of learning functions used. The first group has a discrete set of learning parameters, this is for example the case in linear regression models [33]. The second group has a continuous set of learning parameters which poses a problem in performing the computation in a finite amount of time. In Gaussian process regression (GPR) this problem is tackled by introducing Gaussian probability distributions [48]. This principle has for example been used in models that sample new datapoints based on Bayesian inference, such as Bayesian optimization structure search (BOSS) [49]. Additional control on how the model learns can be exerted by defining other hyperparameters [13, 33].

To train and test the model it is required to use high quality data, with a portion being used for training and a different set being used for validation of the model. It is important for these data sets to not overlap, as that could result in the model training on data that is also used to test it [13, 33]. In the context of catalysis it is also preferable to source experimental data for the model in addition to DFT data in order to let the results better relate to realistic situations [13]. Additionally, care has to be taken in the selection of the size of the data set and how long the model trains in order to avoid over or under fitting, as this can lead to higher errors in the results. However, if the model is well fitted the accuracy is similar to DFT results with a more efficient computation time [33] and making the use of machine learning compelling for complex situations where DFT might require a lot of resources.

2.0.3. Nudged Elastic Band

To find a minimum energy pathway (MEP) between two stable states, or energy minima, and the associated transition state (TS) the Nudged Elastic Band (NEB) method is commonly employed [50, 51]. Examples of transitions were NEB has proven useful is the diffusion of atoms along the surface, or the breaking and forming of chemical bonds [52]. In NEB two stable structures are taken and equally spaced images are created between these two initial states. Additionally, the images have "springs" between them to ensure that the spacing of the images remains approximately equal by applying a restoring force [50]. The structures in the images can then be evaluated and a force can be projected on the potential energy surface (PES) regarding how the structure should change to move towards the minima. The spring force is then projected along the “chain” to ensure spacing whilst the force obtained from the structure is applied perpendicular to the “chain” in order to obtain the structure of the next image to evaluate [50, 52]. In figure 3 this movement is portrayed with the “spring” force preventing the images from

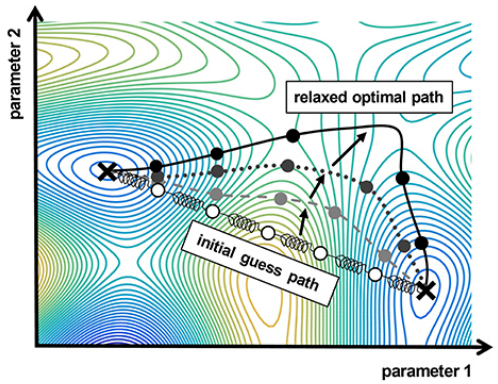

Figure 3: Example progression of equally spaced images towards the minimum energy path during nudged elastic band. The springs between the circles indicate that a spring force is applied to keep the spacing of the images constant. Reprinted with permission from [53].

moving towards the two minima.

With regular NEB it is however likely that the TS is not captured with an image due to their spacing [52], which is also visible in figure 3 with no image on the saddle point. A method to calculate the TS is climbing image NEB (CI-NEB) where the highest energy images, which are likely already close to the TS, have their "springs" removed. These images are then allowed to move up the PES towards the saddle point [51], with the saddle point being a transition state. The removal of these springs increases the degrees of freedom, which makes an initial guess of the MEP required to efficiently reach the saddle point [52].

3. Approach

In this section the details of the calculations and other methods used are explained so that it is clear how the results were obtained. This includes a brief explanation of the parameters used for DFT, NEB and BOSS calculations. A more detailed description of the input files, the keywords and their structures can be found in appendix A. All DFT calculations were performed using the Fritz Haber Institute Ab Initio Molecular Simulations package (FHI-AIMS) [42] with the Perdew-Burke-Ernzerhof (PBE) exchange-correlation [36] functional. CuAu surface slabs consisting of 7 layers and a 15 Å vacuum were based on results from previous work [11, 17], and a Pt coating was added to this surface in this project. The structures of the used Au-terminated and Pt-coated surface are shown in figure 4. The atomic simulation environment (ASE) [52] was used to create new structures and to aid in the visualization of results.

For all performed DFT calculations the atomic zeroth order regular approximation (atomic-ZORA) [42] was employed, which provides a scalar correction to relativistic effects. This was required due to the use of atoms heavier than Ca ($Z > 20$). The self-consistent field (SCF) optimization of the electron density used the Eigenvalue Solvers for Petaflop Applications (ELPA) [54, 55], which improves the performance on high performance computing (HPC) clusters.

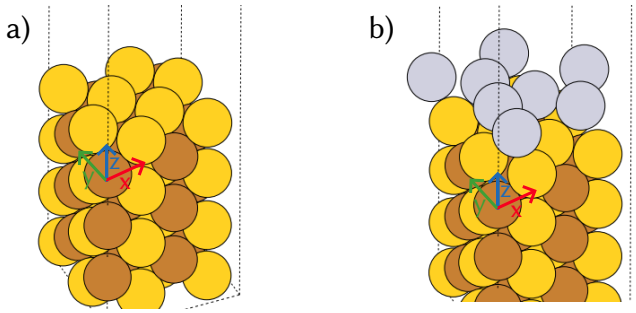

Figure 4: The structures of the two main surfaces used in this work in isometric projection. (a) The Au-terminated surface with 7 metal layers alternating between Au (yellow) and Cu (brown). (b) The Pt (gray) coated surface with 7 metal layers underneath that alternate between Au and Cu.

3.1. Single Point Calculation

Depending on the desired accuracy for the energies, the *light* or *tight* basis sets were used for single point calculations with the pulay mixer [56] and a 12×12×1 k-point grid. For example, the *light* basis set was used for the DFT calculations as part of BOSS or NEB calculations due to *light* calculations being faster. To take spin polarisation into account, collinear spins were set in combination with defining an initial magnetic moment of 1.0 unpaired electron in the structure geometries for the calculation. This initial moment was required to get the spin polarisation started with the eventual spin state distribution being calculated during the SCF cycles.

3.2. Geometry Optimisation

A two-step process was used for all geometry optimizations, with a relaxation with the *light* basis set being followed by one using the *tight* basis set. The determination of the next structure during the relaxation/geometry optimisation was the BFGS method [57]. Other settings for the calculation were kept equal to those described for the single point calculations. During optimisation, some layers of the model were frozen which prevented them from moving during the relaxation steps. Two variants of the base (100) CuAu surface was utilized during these relaxation steps. One where the top 2 metal layers were able to move and the 3 layers underneath were frozen, and one where the top 4 metal layers were able to move with the 2 layers underneath being frozen. Any remaining layers left under the frozen metal layers were also left unfrozen.

3.3. Density of States

The density of states (DOS) for structures was also calculated using FHI-AIMS [42] with a 12×12×12 k-point grid and the *tight* basis set. Additionally, the spin was taken into account as described above. For the output of the DOS, the k-grid was made denser by a factor 12×12×12 to obtain higher accuracy.

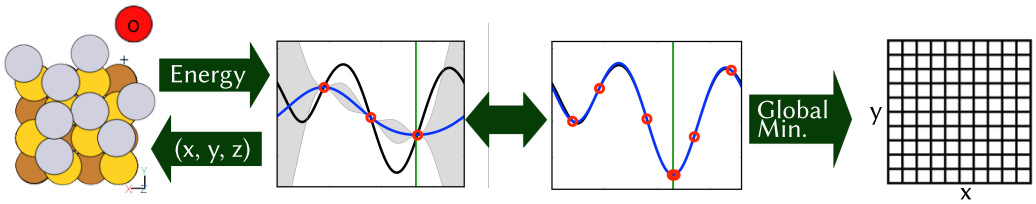

Figure 5: Overview of the adsorption site identification method using Bayesian Optimization Structure Searchboss on a Pt (gray) coated surface with Au (yellow) and Cu (brown) layers underneath. The energy of each configuration is used to determine the parameters of the next sample until the calculated Potential Energy Surface has a low uncertainty. Afterwards a 2D energy map is calculated in the global minimum.

3.4. Adsorption Site Identification

To determine where on a surface a species of interest (such as platinum, or atomic oxygen and hydrogen) might adsorb, the BOSS method [49] and program was used. With it, a surface was sampled using single point calculations within a defined box using the *light* basis set and a 5×5×1 k-point grid. With the BOSS method, 200 initial data points were generated to sample the surface on a mesh, which was followed by at least 50 additional points that were determined using a Bayesian optimisation method [58]. This is a form of machine (accelerated) learning as described in section 2.0.2. One of the obtained outputs from BOSS was a 2D surface energy map at the global minimum, which could be used for further calculations or processing. For diatomic molecules (such as CO) additional rotational variables describing the orientation of the molecule were added, and another BOSS calculation was performed to determine the optimal orientation. The obtained surface energy map was post-processed by subtracting the energy of the components in order to obtain an adsorption energy map. An overview of the described method is shown in figure 5, additional information on the files and keywords for BOSS can be found in appendix A.2.

3.5. Minimum Energy Path & Transition State

To find the MEP between a known initial and final state, such as for the dissociation of oxygen molecules to atomic oxygen on the surface, the NEB method as implemented in ASE [50, 52] was used. Between the initial and final state, 7 images were interpolated and used in the NEB calculations. The energies and forces for each image were obtained using single point calculations using the *light* basis set on a 5×5×1 k-point grid and with a reduced atom count. The new structure for each image was determined in ASE using the Fast Inertial Relaxation Engine (FIRE) method [59, 60] and a convergence criterion of 0.1 eV/Å. This would result in a MEP for the investigated change, but this does not necessarily capture the TS, as discussed in section 2.0.3. To obtain the transition state, another NEB calculation was therefore performed using identical parameters but with the addition of the climbing image (CI) method [51]. The CI-NEB was performed on a 5-image interpolation between two selected structures around the observed energy maximum during regular NEB with a convergence criterion of 0.05 eVÅ. The

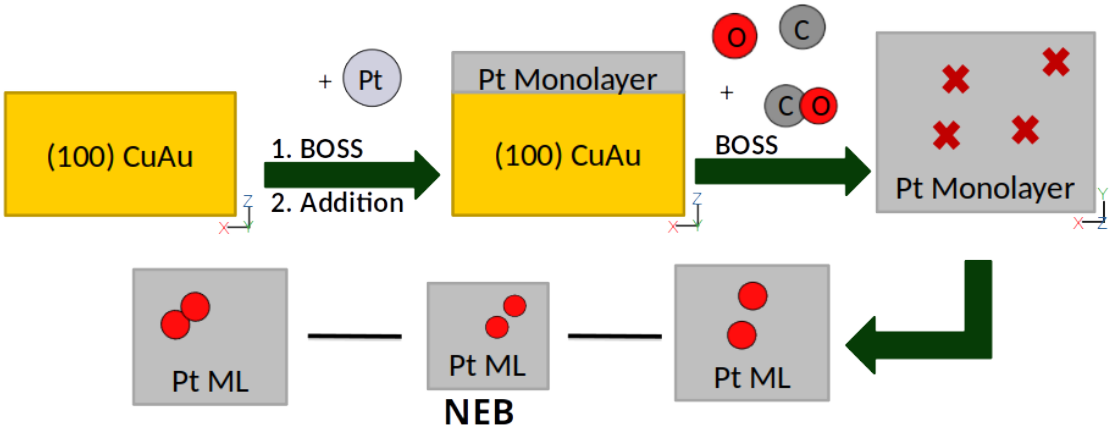

Figure 6: General workflow of the steps taken in the project. Where the adsorption sites were determined using BOSS and the addition of Pt was performed using geometry optimizations. The dissociation of other species (pictured) was performed using Nudged Elastic Band.

obtained TS and minima before the TS were then recalculated using the *tight* basis set to obtain the activation energy and total energy change of the transition.

3.6. General Workflow

The above described methods and parameters were used to perform the calculations for the stated aims of the project. First, the Au-terminated (100) CuAu surface was sampled using BOSS to identify the adsorption sites and compare the used method to intuition and literature, this also allowed for the identification of limitations that BOSS had in the context of the project. With the information on Pt adsorption sites, the surface was filled with a monolayer (ML) of Pt and the associated adsorption energies calculated. From the structures obtained by "filling the surface", one structure was used for further investigations using hydrogen, oxygen and carbon monoxide.

The adsorption and dissociation of H_2, O_2 and CO was investigated by performing BOSS calculations on the Pt-coated surface to identify the adsorption sites. With the adsorption information it was possible to construct initial and final structures for the dissociation of O_2 and H_2. The transition between the molecules and the dissociated atoms could then be analysed using (CI-)NEB to determine the transition states. DOS calculations and a literature review allowed for comparison of the obtained results with known Cu, Au and Pt surfaces. A graphical representation of the described workflow is shown in figure 6.

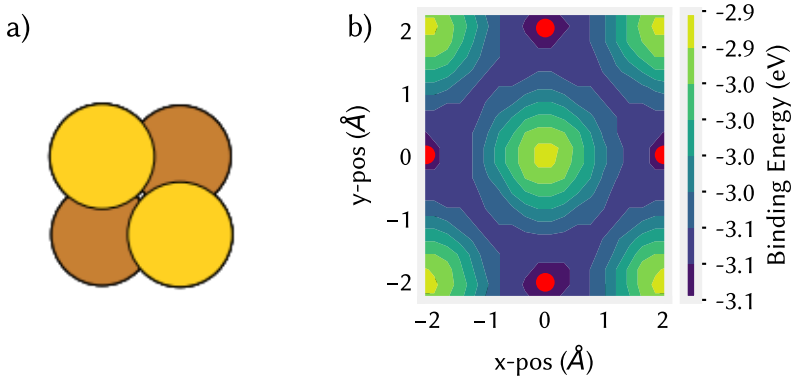

Figure 7: (a) Structure of the Au-terminated (100) CuAu surface that was sampled using Bayesian Optimization Structure Search (BOSS), with the terminal Au atoms (yellow) and sub-surface Cu atoms (brown) shown. (b) The obtained 2D adsorption energy map at the global minimum from BOSS. The positions of the Au atom are marked with red dots in the energy map.

4. Results & Discussion

With CuAu surfaces forming the starting point of the thesis, the first step is to identify the Pt adsorption sites and add 1 monolayer of Pt on the Au-terminated (100) CuAu surface. The resulting surface(s) can then be used to investigate the adsorption and dissociation of O_2 and H_2 on the coated surface.

4.1. Pt adsorption sites

To determine the adsorption sites of Pt on an Au-terminated (100) CuAu surface slab, the BOSS method [49] was employed as described in section 3.4. With this method the surface with 4 terminal Au atoms (Figure 7a) was sampled using a single Pt atom in a 3.0 Å high box located 0.4 Å above the centre of the terminal Au atoms. Once the BOSS process was finished the resulting 2D surface energy map was used to obtain a binding energy map with separate single point calculations of the components (Pt and the surface in this case). The binding energy map (Figure 7b) has a z-coordinate of 2.8 Å above the Au atom centres, which indicates that at this height the individual Pt atoms prefer to adsorb on the top sites of the Au atoms.

This adsorption site was different from the expected behaviour from the literature and could, in part, be due to how the sampling is performed using BOSS. Since BOSS, in this case, sampled with simple single point calculations and with no regard for the centres of other atoms when selecting the next sample location it was required to choose an lower boundary that would not result in the Pt atom clashing with the Au atom. This requirement therefore introduced a certain amount of bias for positions further away from the surface.

A possible way to obtain a surface energy map (as shown in Figure 7) that also samples the hollow sites and stepped sites, such as a (211) surface slab, without the above mentioned problem would be an alteration to the user function in how it received and supplied positional and energy data from and to BOSS. A different alternative would be the usage of other tools,

such as Ab initio random structure searching (AIRSS) [61] or Atomistic Global Optimization X (AGOX) [62] that performs smart sampling using a Guassian Process Regression Model but has been shown to be able to sample the configuration of 14 Pt atoms on a bulk Au surface where the boundary extends into the said surface.

4.2. Addition of Pt to the surface

To obtain a Pt-coated surface the obtained Pt adsorption sites are used to fill the 'bare' Au-terminated surface. This filling was performed using three different techniques, with the first two consisting of bringing 6 or 8 Pt atoms close to the surface as a monolayer or cluster and performing a relaxation of the structure. The third and main method consists of adding the Pt atoms sequentially and performing a full relaxation cycle (with *light* , followed by *tight* basis set relaxation). This sequential filling was performed at least twice for each added Pt to obtain a wider spread in possible configurations and energies of the Pt-coated surface. Using *tight* basis set calculations of the components for Pt filling (the surface and Pt atom) it was possible to calculate and plot the adsorption energy (Figure 8) after each relaxation cycle using the equation $E_{ads} = E_{CuAu+nPt} - (E_{CuAu} + nE_{Pt})$.

The Pt atoms were added to the surface on the top and hollow sites following the initial addition on only the top sites. The initial addition to the top site quickly showed that the Pt atoms will relax towards the hollow sites (in addition to the Au atoms moving around to accommodate). This movement towards the hollow site is in agreement with the earlier discussion regarding the BOSS results (Figure 7) where Pt was found to adsorb on the top site. Additionally, the layered structure of the surface remained during the adsorption (Figure 9c) as a consequence of the DFT calculations being performed in a vacuum at 0 K [7].

From the plot in figure 8 where up to 8 Pt atoms were added to the surface a clear downwards trend is visible where more added Pt atoms on the surface result in a lower and more favourable binding energy. This indicates that the addition of Pt on this surface will result in a fully covered surface. Literature on CuAu or Au clusters with Pt show that the terminus of the structure is in part determined by the ratios of the Cu, Au and Pt atoms [21, 24] with the abundant atom forming the outer shell. This trend can be partially explained by the outer shell requiring more atoms to fully cover than internal layers. However, such mixing would require some external energy (heat) to facilitate. Our computations correspond to the case where previously synthesised CuAu clusters are coated with Pt. To investigate if these structures are stable over a longer time, a follow up study is required where, for example, molecular dynamics simulations are performed to introduce temperature.

To construct the plot in figure 8, two different Au-terminated (100) CuAu surfaces with one having 2 and the other having 4 *surface layers*. The surface layer count indicates how many layers of the surface are unconstrained and are thus able to move during the relaxation. For the 2 *surface layer* (2SL) samples only the top Au and underlying Cu layer are able to move with lower layers being frozen. The 4 *surface layer* (4SL) plot on the other hand had an additional Au and Cu layer that can move during relaxation. In figure 8 the energy of both approaches converges towards a similar value with the 4SL samples having a slightly more favourable energy due to the increased freedom. Despite the similar energy, the structure when 8 Pt atoms are added to the surface is different (Figure 9) due to the higher flexibility of the 4SL sample.

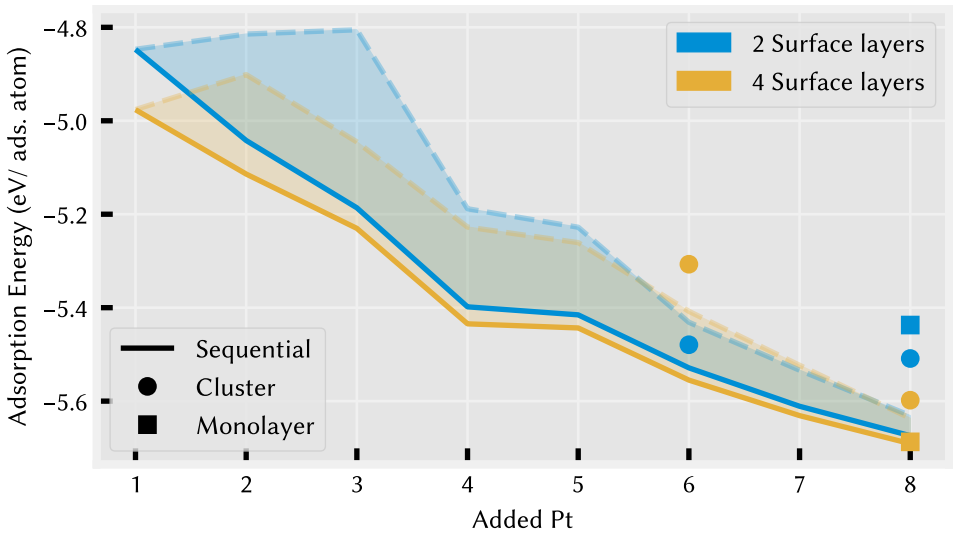

Figure 8: Calculated adsorption energy of Pt on Au-terminated (100) CuAu with an increasing number of Pt atoms on the surface. The adsorption energy was calculated using $E_{ads} = E_{CuAu+nPt} - (E_{CuAu} + nE_{Pt})$. The results for two series of calculations are shown. In the first series two CuAu surface layers relaxed together with the Pt atoms (blue), whilst the second series four CuAu layers were relaxed (yellow). The solid lines indicate the adsorption energies of the most favourable adsorption sites, with the shaded areas indicating the energies of all other configurations. For 6 and 8 adsorbed Pt atoms, the energies of monolayer structures (square symbols) are also compared with those of adsorbed Pt clusters (circles).

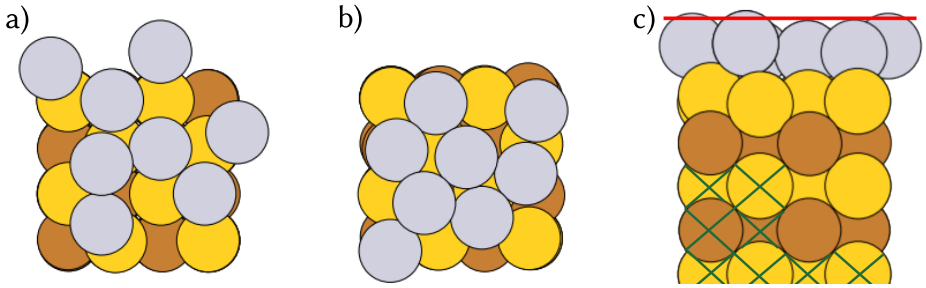

Figure 9: Top view of the surface for Pt addition on (a) 2 surface layers and (b) 4 surface layers. The Pt atoms (gray) form the top layer with Au (yellow) and Cu (brown) underneath. The impact that more relaxed layers during sequential addition can have is visible. (c) Side view of the coated surface in (a) that illustrates the difference between 2 (left half) and 4 (right half) surface layers with the frozen atoms marked with green crosses. Additionally, an xy plane is visible in red, showing the unevenness of the coated surface. The energies of the structures are incorporated in the plot in figure 8.

For the investigations into the dissociation of O_2 and H_2, and the adsorption of C and CO on the Pt-coated surface it was decided that the 2SL structure shown in figure 9 would be used. This was partly done due to this structure being available earlier for the required calculations. Additionally it was reasoned that the structure of a Pt-coated NP would likely not conform to the near perfect structure seen in the 4SL sample (Figure 9).

4.3. Adsorption sites on Pt-coated surface

The dissociation of species on the Pt-coated surface was investigated using NEB calculations. However, these calculations require a static or known initial and final structure between which the NEB images are made. Instead of sampling various areas of the surface by hand the surface was sampled using the mono- and diatomic molecules of interest with BOSS as described in sections 3.4 and 4.1.

4.3.1. Oxygen and Hydrogen

The first two species of interest to be sampled were atomic oxygen and hydrogen. For oxygen the sampling using BOSS resulted in a 2D energy map that had a z-coordinate 2.0 Å above the centre of the Pt atoms of the surface and with the adsorption energies calculated (Figure 10a). The figure obtained using BOSS sampling shows that for atomic oxygen the most favourable binding positions are the bridge sites with some broadening towards the hollow sites. The adsorption sites found using BOSS agree with the literature result for (100) Au-Pt [19]. Similar results were found for (100) Pt-coated surfaces were the subsurface layers consisted of Cu and pure Pt [22, 29]. In contrast the (100) Au surface was found to have preferable binding of atomic oxygen on the hollow sites [28], indicating that the adsorption of species is closely linked to the

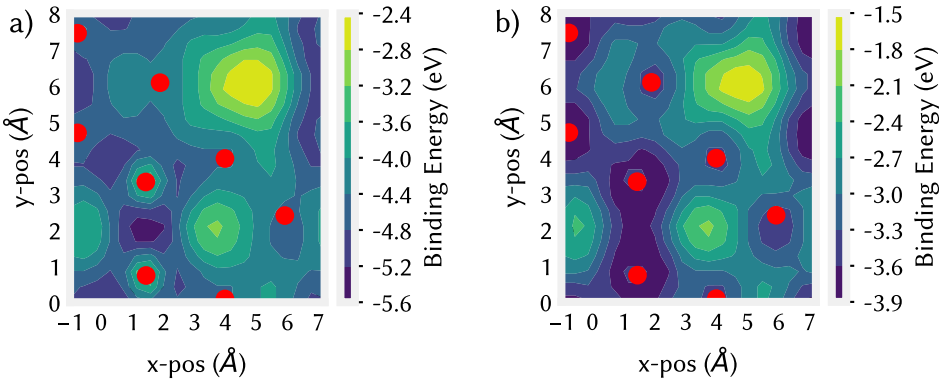

Figure 10: 2D Surface energy maps of atomic (a) O and (b) H using Bayesian Optimization Structure Search on the Pt-coated surface (Figure 9a). The lowest energy regions, which are most favourable for binding, are coloured in blue and the Pt atom positions are marked with red dots.

surface composition [9]. Literature on molecular oxygen indicates that the preferable binding site was the bridge position with both oxygen atoms located towards the top sites on (111) Pt [22, 28].

A notable trend visible in the obtained results from BOSS is that the energy generally seems to increase if the oxygen is farther removed from the Pt atoms, for example around (x,y)=(5,6) (Figure 10a), or when the oxygen gets right on top of the Pt atoms. This latter trend for when the oxygen is located on top of the Pt does however see large variability in the actual increase, which could in part be due to the Pt atom positions not having an identical z-value and them being merely close to the same xy-plane (Figure 9 right). Plotting this 2D plane/energy map through the global minimum on this slightly uneven surface likely resulted in some positions having a different perceived energy. This is in some ways similar to the lower bounds issue mentioned in section 4.1. The surface used for oxygen adsorption was also used for hydrogen and carbon monoxide, with similar complications being seen.

For hydrogen the obtained 2D surface energy map is shown in figure 10b and the 2D plane for this species was located 1.8 Å above the Pt atoms of the surface. From the figure it can be seen that the most favourable adsorption site is the bridge site with the top site being $\leq$1 eV less stable. These site preferences differ from those found in literature for a (100) and (110) pure Pt surface in vacuum, where a hollow site was the most favourable [63] instead of the bridge site, which was found to be a primary adsorption site in an aqueous environment [64]. Both the literature and thesis results indicate, however, that the bridge site is a possible binding location for hydrogen atoms [63]. The obtained energy map and literature insights were used to construct possible initial and final configurations for the investigation of the dissociation using NEB.

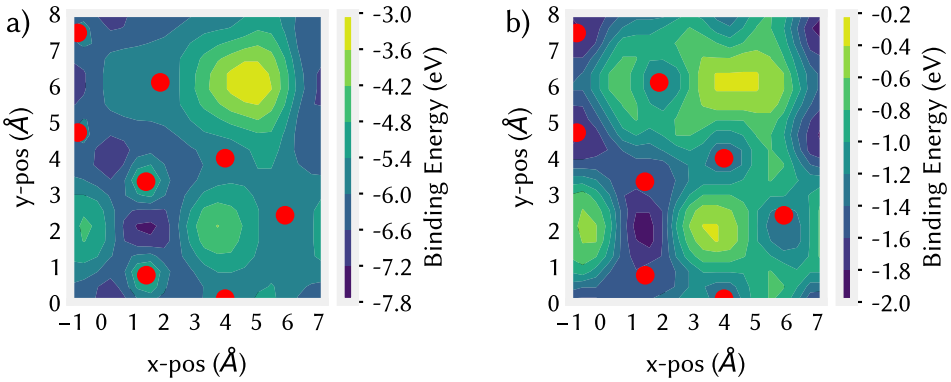

Figure 11: 2D Surface energy maps of (a) atomic C and (b) molecular CO without rotational freedom using BOSS on the Pt-coated surface (Figure 9a). The lowest energy regions, which are most favourable for binding, are coloured in blue and the Pt atom positions are marked with red dots.

4.3.2. Carbon and Carbon Monoxide

To investigate the dissociation of CO on the surface, additional BOSS calculations for carbon and carbon monoxide were required. In addition to the positional variables (x,y,z) used for oxygen and hydrogen, the CO molecule required rotational parameters due to its degrees of freedom. The rotation was incorporated in a separate calculation after the position was determined. The obtained adsorption energy map using BOSS for atomic C and molecular CO are in figure 11, the rotational energy map for CO can be found in appendix C.

From the BOSS calculations it was found that atomic C has preference for adsorption on the bridge sites between Pt atoms. The CO molecule also shows this preference, but has the top site of the Pt atoms as a secondary adsorption position. The CO molecule was adsorbed with the carbon atom closest to the surface, while it was found that CO adsorbs on the top site for pure Pt [65] and AuPt clusters [23]. This difference could be due to the most active facet of the Pt cluster not being a (100) surface or the subsurface Au and Cu atoms in the trimetallic surface influencing the CO adsorption characteristics.

4.4. Dissociation of O_2

For the dissociation of oxygen on the Pt-coated surface, the adsorption results found using BOSS (section 4.3.1) were used in addition to literature information regarding the adsorption of O_2. With the aforementioned resources the likely sites were identified as a bridge site for the initial position of O_2 [22, 28, 30] and a bridge or hollow site for the final position. To obtain the used initial and final positions a geometry optimisation using the *light* basis set was performed on the likely positions in order to account for changes in the surface structure due to the added atoms. This resulted in the O_2 molecule for the initial position being adsorbed on the bridge site, and the 2 oxygen atoms located in a hollow site with the Pt atoms rearranging slightly to form FCC-like hollows with the Pt atoms forming rough triangles.

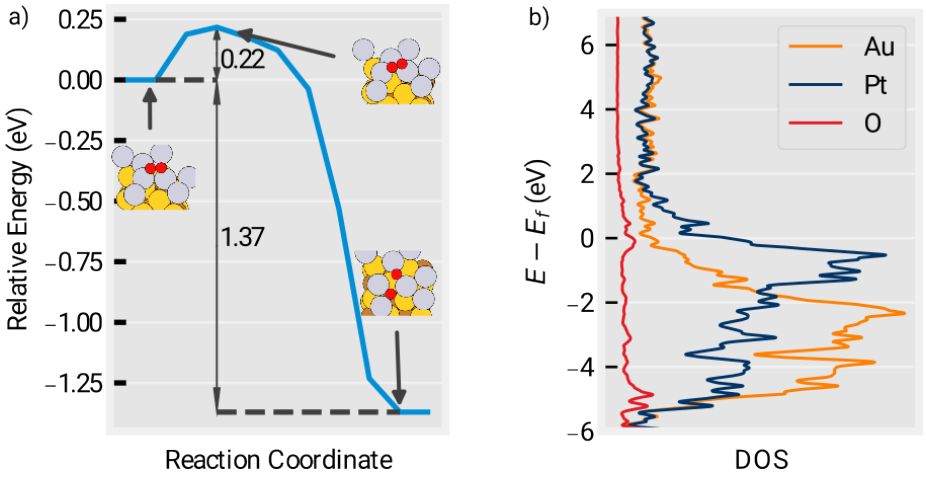

Figure 12: Dissociation of O_2 on a Pt-coated (100) CuAu surface. (a) The energy plot obtained using (Climbing Image-)Nudged Elastic Band calculations, with the initial, final and TS structures shown. (b) The species-projected and spin-polarised Density of States of the top 2 layers and oxygen. E_f is the Fermi energy.

With the obtained initial and final structures NEB calculations were performed using 7 interpolated images, followed by CI-NEB around the highest energy states using 5 interpolated images. The resulting MEP and TS could then be plotted in figure 12a. The NEB plot, where the structures of the minima before and after the TS are shown, indicates that the activation energy for the dissociation of O_2 on this surface is 0.22 eV. This relatively low barrier agrees with findings in the literature where the activation barrier was reported to be low at low oxygen surface coverage [30] with DFT observed values between 0.05 and 0.13 eV for (100) Pt and Cu/Pt [22, 28] and an experimental value of 0.36 eV for (111) Pt [28]. As such, the calculated CuAU/Pt structure is close in TS energy to reported pure Pt structures and significantly lower compared to a pure Au structure (0.44 eV) [28]. Additionally, the almost negligible energy barrier found on Cu/Pt hints at the interaction between a Cu-terminated structure having a better interaction with the Pt atoms, though further calculations might be required to confirm or refute this. The total energy change in the model due to the dissociation, or the reaction energy, was calculated to be -1.36 eV. This result for the trimetallic CuAu/Pt system was similar to the -1.32 and -1.28 eV reaction energies found for (100) Cu/Pt and (100) Pt in literature [22]. The obtained results for the TS and reaction indicate that the dissociation should be energetically highly favourable and relatively easy, with the surface layer likely contributing most to the characteristics.

Further insight on the binding of the species on the surface can be obtained from density of states (DOS) calculations. Calculating the species projected DOS on the spin-polarised system before dissociation for the top surface layers resulted in the plot shown in figure 12 right. The spin polarisation did not appear to result in different DOS positions for the spin up and down densities when Au is included, appendix B shows that for DOS on samples with only Pt and oxygen there is an observable effect. Notable is the proximity of the Pt density to 0 eV, i.e., the Fermi energy, which has been correlated to a higher surface reactivity with diatomic molecules

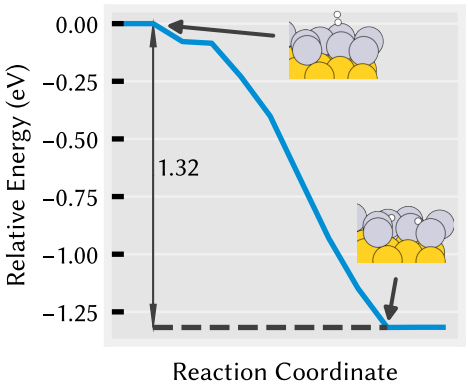

Figure 13: Energy plot for the dissociation of H_2 using (Climbing Image-)Nudged Elastic Band with the initial and final structures shown.

(such as O_2) [9, 23]. This effect has been attributed to strain caused by the subsurface layers on the top layer of the surface, which would for this surface be the strain in the Pt caused by the CuAu bulk underneath. Another notable aspect of the DOS is the position of the main oxygen π bonding contribution at 0 eV showing an overlap with the main surface contribution from Pt compared to the significantly wider gap observed for Au-terminated surfaces [11]. This indicates, in agreement with the observed adsorption energies, that the adsorption of oxygen on the Pt-coated surface is facile.

4.5. Dissociation of H_2

The dissociation of hydrogen was investigated in a similar manner to oxygen (section 4.4) with the initial and final configuration being selected using the results from BOSS and the literature (section 4.3.1), and all structures were again optimised using the *light* basis set. The bridge and top sites were used to obtain a final structure and once geometry optimisation was completed the structure had one hydrogen atom on an fcc-like hollow site and the second atom on a bridge site between two Pt atoms. A stable initial structure of H_2 on the surface was impossible to obtain due to the extremely low dissociation barrier for hydrogen on a clean surface [66]. A stable initial structure was obtained when the H_2 molecule was located 2.4 Åfrom the surface. The obtained results from the NEB and CI-NEB calculation for the selected initial and final structures are shown in figure 13 where the dissociation had an energy difference of 1.32 eV. The main notable feature from this plot is the lack of a transition state, indicating that the dissociation occurs spontaneously. This was observed in the literature for clean surfaces with <0.5 ML of hydrogen coverage [66].

5. Conclusion

A Pt-coated CuAu surface was successfully constructed from an Au-terminated (100) CuAu base surface using DFT with the PBE functional. The constructed surfaces were observed to have varying configurations despite similar total structure energies, with the Pt atoms being observed on the hollow sites and displaced towards the on-top sites. This difference in configuration was attributed to the used adsorption positions of Pt on the surface with addition on sites with a higher degree of freedom resulting in rougher surfaces. Furthermore, the addition of Pt to the surface resulted in the formation of at least a single monolayer of Pt atoms.

Afterwards, the adsorption sites for atomic oxygen, hydrogen and carbon, and molecular CO were determined on a Pt-coated surface using BOSS. It was found that atomic oxygen and hydrogen adsorb on the hollow sites and to a lesser extend the bridge sites, with molecular oxygen adsorbing on the bridge site with an adsorption energy of -2.24 eV. Atomic carbon adsorbs on the bridge site. Molecular hydrogen was found to adsorb dissociatively on the clean surface, and CO molecules adsorb on the bridge or top sites. Based on DOS calculations, the favourable adsorption of oxygen was hypothesised to likely be caused by strain in the Pt layer increasing the energy of the Pt band and the overlap with the oxygen bonding states. The dissociation of O_2 and H_2 was investigated using NEB calculations between the determined states before and after dissociation. With these NEB calculations the activation energy of the oxygen dissociation was found to be 0.22 eV, whilst the hydrogen dissociation would occur spontaneously with no noticeable energy barrier. These results were in agreement with existing research on mono- and bimetallic Pt surfaces for oxygen and hydrogen adsorption and dissociation, suggesting that the main contributor to the activity is the surface composition.

6. Outlook

During the project, the scope of the surface was limited to only the (100) Au-terminated surface, due to Au being a known terminus in a vacuum, resulting in insights into the Pt-coated surface on only a single type of facet. As such, it is encouraged to also investigate different facets such as the (111) or (211) facet to get a wider understanding of the effect that CuAu may have on the Pt shell compared to, for example, just copper or gold. This would also increase the scope of a DFT database when a machine learning model is made for the trimetallic system. Additionally, the structures can also be investigated using molecular dynamics to simulate the particle at temperatures above the 0 K used in regular DFT, with the above mentioned possibilities contributing to a better understanding of a realistic particle.

Expanding the investigated reactions on the surface would also be beneficial to gain a better understanding of the activity of this trimetallic particle for different base reactions. A possible angle to take in order to further understand the underlying mechanisms to the changes in activity would also be the strain in the surface, which was only briefly mentioned based on literature. This would also be well served to combine with experimental endeavours into synthesising and analysing the trimetallic CuAu/Pt NP. An experimental investigation into such effects is currently an ongoing project in Dr. Jessi van der Hoeven's group.

7. Acknowledgements

Dr. N. Artrith is thanked for providing the daily supervision throughout the project in addition to serving as the first examiner. This includes her enthusiastic introduction to the broader subject of computational chemistry sparking the start of this project, and commentary on various research ideas. Valuable guidance and feedback on the presentations, this thesis and scientific poster has also been provided and has been of significant help in improving my scientific communication. Finally, the help in finding an internship after the project is greatly appreciated.

Prof. Dr. F.M.F. de Groot is thanked for being the second examiner of the project, suggesting literature and sharing information during the theory group meetings. Dr. J. van der Hoeven is thanked for providing the collaboration that sparked this computational project into existence, and Prof. Dr. P.E. de Jongh is thanked for leading the Materials Chemistry and Catalysis group and therefore making this project possible.

Current and former members of the theory group are thanked for their feedback, beneficial discussions and sharing of information. L. Ngamwongwan and K. Rommens are thanked for their support in setting up the software and scripts for the Snellius HPC, with additional thanks to R. García-Muelas for providing further support during nudged elastic band calculations. M. Rokhline, J. He and W. van Weesep and the other members of the theory group thanked for their feedback and wished good luck in their continued research.

The computational resources on National Supercomputer Snellius, provided by SURF, and Aenetone, with technical support by Ing. C.G. van der Werf of the Faculty of Science, are gratefully acknowledged in making the project possible.

The entire MCC group is thanked for providing a welcoming and stimulating work and social environment, and for organizing various group activities to connect the members of the group.

Finally, the reader is thanked for the interest in the project subject and taking the time to read this thesis.

8. List of Abbreviations

ASE	Atomic Simulation Environment
BOSS	Bayesian Optimization Structure Search
CI-NEB	Climbing Image Nudged Elastic Band
DFT	Density Functional Theory
DOS	Density of States
FCC	Face Centered Cubic
GGA	Generalized Gradient Approximation
HPC	High Performance Cluster
KS	Kohn-Sham
LDA	Local Density Approximation
MEP	Minimum Energy Pathway
ML	Monolayer
MOR	Methanol Oxidation Reaction
NAO	Numeric Atom-centered Orbitals
NEB	Nudged Elastic Band
NP	Nanoparticle
ORR	Oxygen Reduction Reaction
PES	Potential Energy Surface
SL	Surface Layer
TS	Transition State
XC	Exchange and Correlation

References

[1] C. G. Morales-Guio, E. R. Cave, S. A. Nitopi, J. T. Feaster, L. Wang, et al., *Nature Catalysis* **2018**, *1*, 764–771.

[2] T. Xue, C. Wu, X. Ding, J. Sun, *Physical Chemistry Chemical Physics* **2018**, *20*, 17927–17933.

[3] C. Wang, D. van der Vliet, K. L. More, N. J. Zaluzec, S. Peng, et al., *Nano Letters* **2011**, *11*, 919–926.

[4] J. Brindle, M. M. Nigra, *ACS Omega* **2021**, *6*, 24269–24279.

[5] R. Prins, A. Wang, X. Li, *Introduction to Heterogeneous Catalysis*, *Vol. 2*, WORLD SCIENTIFIC (EUROPE), **2016**.

[6] R. Ferrando, J. Jellinek, R. L. Johnston, *Chemical Reviews* **2008**, *108*, 845–910.

[7] J. M. Rahm, P. Erhart, *The Journal of Physical Chemistry C* **2018**, *122*, 28439–28445.

[8] Y. Xu, A. V. Ruban, M. Mavrikakis, *Journal of the American Chemical Society* **2004**, *126*, 4717–4725.

[9] J. Niemantsverdriet, I. Chorkendorff, "Surface Reactivity" in *Concepts of Modern Catalysis and Kinetics*, John Wiley & Sons, Ltd, **2003**, pp. 215–266.

[10] K. Loza, M. Heggen, M. Epple, *Advanced Functional Materials* **2020**, *30*, 1909260.

[11] N. Artrith, A. M. Kolpak, *Nano Letters* **2014**, *14*, 2670–2676.

[12] C. Li, S. Yan, J. Fang, *Small* **2021**, *17*, 2102244.

[13] N. Artrith, *Matter* **2020**, *3*, 985–986.

[14] C. Romainczyk, J. R. Manson, K. Kern, K. Kuhnke, R. David, et al., *Surface Science* **1995**, *336*, 362–370.

[15] J. Niemantsverdriet, I. Chorkendorff, "Solid Catalysts" in *Concepts of Modern Catalysis and Kinetics*, John Wiley & Sons, Ltd, **2003**, pp. 167–214.

[16] X. Sun, D. Li, Y. Ding, W. Zhu, S. Guo, et al., *Journal of the American Chemical Society* **2014**, *136*, 5745–5749.

[17] N. Artrith, A. M. Kolpak, *Computational Materials Science* **2015**, *110*, 20–28.

[18] D. S. He, Y. Han, J. Fennell, S. L. Horswell, Z. Y. Li, *Applied Physics Letters* **2012**, *101*, 113102.

[19] S. Jalili, A. Zeini Isfahani, R. Habibpour, *Computational and Theoretical Chemistry* **2012**, *989*, 18–26.

[20] H. B. Liu, U. Pal, J. A. Ascencio, *The Journal of Physical Chemistry C* **2008**, *112*, 19173–19177.

[21] L. Vega Dominguez, H. A. Aleksandrov, R. Farris, A. Bruix, F. Viñes Solana, et al., **2021**.

[22] K. Li, Y. Li, Y. Wang, F. He, M. Jiao, et al., *Journal of Materials Chemistry A* **2015**, *3*, 11444–11452.

[23] D. Mott, J. Luo, P. N. Njoki, Y. Lin, L. Wang, et al., *Catalysis Today* **2007**, *122*, 378–385.

[24] G. Wu, Y. Sun, X. Wu, R. Chen, Y. Wang, *Chemical Physics Letters* **2017**, *686*, 103–110.

[25] J. W. M. Crawley, I. E. Gow, N. Lawes, I. Kowalec, L. Kabalan, et al., *Chemical Reviews* **2022**, *122*, 6795–6849.

[26] J. Yang, X. Chen, X. Yang, J. Y. Ying, *Energy & Environmental Science* **2012**, *5*, 8976–8981.

[27] P. C. Jennings, H. A. Aleksandrov, K. M. Neyman, R. L. Johnston, *Nanoscale* **2014**, *6*, 1153–1165.

[28] M. M. Montemore, M. A. van Spronsen, R. J. Madix, C. M. Friend, *Chemical Reviews* **2018**, *118*, 2816–2862.

[29] R. Li, H. Li, J. Liu, *International Journal of Quantum Chemistry* **2016**, *116*, 908–914.

[30] S. Yotsuhashi, Y. Yamada, T. Kishi, W. A. Diño, H. Nakanishi, et al., *Physical Review B* **2008**, *77*, 115413.

[31] J. K. Nørskov, F. Abild-Pedersen, F. Studt, T. Bligaard, *Proceedings of the National Academy of Sciences* **2011**, *108*, 937–943.

[32] W. Kohn, L. J. Sham, *Physical Review* **1965**, *140*, A1133–A1138.

[33] L. Fiedler, K. Shah, M. Bussmann, A. Cangi, *Physical Review Materials* **2022**, *6*, 040301.

[34] N. Mardirossian, M. Head-Gordon, *Molecular Physics* **2017**, *115*, 2315–2372.

[35] O. Y. Long, G. Sai Gautam, E. A. Carter, *Physical Review Materials* **2020**, *4*, 045401.

[36] J. P. Perdew, K. Burke, M. Ernzerhof, *Physical Review Letters* **1996**, *77*, 3865–3868.

[37] J. Sun, A. Ruzsinszky, J. P. Perdew, *Physical Review Letters* **2015**, *115*, 036402.

[38] J. W. Furness, A. D. Kaplan, J. Ning, J. P. Perdew, J. Sun, *The Journal of Physical Chemistry Letters* **2020**, *11*, 8208–8215.

[39] P. E. Blöchl, *Physical Review B* **1994**, *50*, 17953–17979.

[40] G. Kresse, J. Furthmüller, *Computational Materials Science* **1996**, *6*, 15–50.

[41] P. Giannozzi, O. Andreussi, T. Brumme, O. Bunau, M. B. Nardelli, et al., *Journal of Physics: Condensed Matter* **2017**, *29*, 465901.

[42] V. Blum, R. Gehrke, F. Hanke, P. Havu, V. Havu, et al., *Computer Physics Communications* **2009**, *180*, 2175–2196.

[43] A. Chandrasekaran, D. Kamal, R. Batra, C. Kim, L. Chen, et al., *npj Computational Materials* **2019**, *5*, 22.

[44] N. Artrith, Z. Lin, J. G. Chen, *ACS Catalysis* **2020**, *10*, 9438–9444.

[45] R. Car, *Nature Chemistry* **2016**, *8*, 820–821.

[46] A. Jain, S. P. Ong, G. Hautier, W. Chen, W. D. Richards, et al., *APL Materials* **2013**, *1*, 011002.

[47] T. Mitchell, *Machine Learning*, 1st, McGraw-Hill, **1997**, 432 pp.

[48] C. E. Rasmussen, C. K. I. Williams, *Gaussian Processes for Machine Learning*, The MIT Press, **2005**.

[49] M. Todorović, M. U. Gutmann, J. Corander, P. Rinke, *Npj computational materials* **2019**, *5*, 35.

[50] G. Henkelman, H. Jónsson, *The Journal of Chemical Physics* **2000**, *113*, 9978–9985.

[51] G. Henkelman, B. P. Uberuaga, H. Jónsson, *The Journal of Chemical Physics* **2000**, *113*, 9901–9904.

[52] A. Hjorth Larsen, J. Jørgen Mortensen, J. Blomqvist, I. E. Castelli, R. Christensen, et al., *Journal of Physics: Condensed Matter* **2017**, *29*, 273002.

[53] C. Tönsing, J. Timmer, C. Kreutz, *Frontiers in Physics* **2019**, *7*.

[54] V. W.-z. Yu, F. Corsetti, A. Garcia, W. P. Huhn, M. Jacquelin, et al., *Computer Physics Communications* **2018**, *222*, 267–285.

[55] A. Marek, V. Blum, R. Johanni, V. Havu, B. Lang, et al., *Journal of Physics: Condensed Matter* **2014**, *26*, 213201.

[56] P. Pulay, *Chemical Physics Letters* **1980**, *73*, 393–398.

[57] "Quasi-Newton Methods" in *Numerical Optimization*, (Eds.: J. Nocedal, S. J. Wright), Springer New York, New York, NY, **2006**, pp. 135–163.

[58] M. U. Gutmann, J. Cor, er, *Journal of Machine Learning Research* **2016**, *17*, 1–47.

[59] E. Bitzek, P. Koskinen, F. Gähler, M. Moseler, P. Gumbsch, *Physical Review Letters* **2006**, *97*, 170201.

[60] D. Sheppard, R. Terrell, G. Henkelman, *The Journal of Chemical Physics* **2008**, *128*, 134106.

[61] C. J. Pickard, R. J. Needs, *Journal of Physics: Condensed Matter* **2011**, *23*, 053201.

[62] M.-P. V. Christiansen, N. Rønne, B. Hammer, *Journal of Chemical Physics* **2022**, *157*, 054701.

[63] C. D. Vurdu, *Advances in Condensed Matter Physics* **2018**, *2018*, 1–10.

[64] J. A. Santana, J. J. Saavedra-Arias, Y. Ishikawa, *Electrocatalysis* **2015**, *6*, 534–543.

[65] R. de Souza Monteiro, L. W. C. Paes, J. W. de M. Carneiro, D. A. G. Aranda, *Journal of Cluster Science* **2008**, *19*, 601–614.

[66] A. A. Koverga, E. Flórez, C. Jimenez-Orozco, J. A. Rodriguez, *Physical Chemistry Chemical Physics* **2021**, *23*, 20255–20267.

[67] C. G. Broyden, *Mathematics of Computation* **1965**, *19*, 577–593.

Appendices

A. Computation Input Files

A.1. Frits Haber Institut - Ab Initio Molecular Simulations (FHI-AIMS)

`geometry.in` file The `geometry.in`, with an example being shown in figure 1, contains the positions of the atoms and the shape of the simulation cell if periodic calculations are performed. This shape, or unit cell, is defined by setting the lattice vectors using the keyword `lattice_vector`. The position of an atom is defined by using the keyword `atom`, followed by the coordinate numbers and the element. If a spin-polarized calculation is performed it is required that at least one atom has a defined intiial spin with the `initial_moment` keyword. The relaxation of an atom can be constrained by writing `relaxation_constraint .true.` under the atom that should be constrained. Constraining, or freezing, the atom during relaxation prevents it from moving at all and can serve as a static anchor during relaxations.

```
lattice_vector  4.0445  0.0000  0.0000
lattice_vector  -0.0016  4.0445  0.0000
lattice_vector  0.0000  0.0000  28.2869
atom  0.0116  0.0116  7.3290  Cu
     constrain_relaxation  .true.
atom  2.0334  0.0106  9.1579  Au
     constrain_relaxation  .true.
atom  0.0110  0.0110  10.9439  Cu
atom  2.0331  0.0110  12.6873  Au
```

Listing 1: Example of a geometry input file that contains a unit cell and constrained atoms.

`control.in` file The `control.in`, with an example being shown in listing 2, contains all the keywords and descriptions of the system. With the contents ranging from the XC functional (`xc`) and treatment of relativistic effect, to geometry optimization (`relax_geometry`) and the convergence criteria. Furthermore, smearing functions like Gaussian can be used to control the electronic occupation. To aid convergence of the self-consistent field (scf) cycle different mixers are available like Linear, Broyden [67] or Pulay [56], with the latter being de default and generally recommended. For periodic systems it is required to, in addition to the lattice vectors in `geometry.in`, define the definition of a k-point grid in this file.

The `control.in` also contains the basis set functions of each species present in a given calculation, with the standard procedure suggesting that one copies the basis sets for an element that is provided by FHI to the `control.in` file. For each species three different basis sets were defined in advance [42], with the first small basis set containing just the minimal basis consisting of the just the occupied orbitals and a few additional orbitals. This basis set is called the *light* setting with the second basis sets being called the *tight* basis set. The latter generally gives converged results in the meV-range for the absolute energies and due to this these sets are generally used to check results obtained from *light* settings and further relax a structure after pre-relaxation has finished. The third basis sets are called *really-tight* and should generally only

be used to verify results from calculations using *tight* or if tigher convergence is desired, due to the *tight* basis sets being strongly converged already.

```
#  Physical model settings
  xc                pbe
  vdw_correction_hirshfeld
  charge            0.
  spin              none
  relativistic      atomic_zora scalar
#  SCF convergence settings
  occupation_type   gaussian 0.1
  mixer             pulay
#  Periodic Boundary Conditions
  k_grid            12 12 1
```

Listing 2: Example of the control input file used for geometry optimizations. The basis set was generally also included after the

A.2. Bayesian Optimization Structure Search

Bayesian Optimization Structure Search (BOSS)[49] is a computational tool that can be used for global structure search based on user created "building blocks". It employs Bayesian Optimization [58], which is based on Gaussian Process regression [48], to generate surrogate models for selected properties using the given data that is obtained from atomistic simulations or DFT. The used program was a python package named `aalto-boss` and was provided under the BSD-3 license by the Computational Electronic Structure Theory group at Aalto University. For basic running of the program on HPCś it required three files to be present in the working directory: a `boss.in` file, and a `userfn.py` and starting bash script. The name of `userfn.py` can by anything, but needs to be defined in `bos.in`.

The DFT calculations that provide the data for the surrogate model were performed using the *light* basis set for FHI-AIMS with a 5x5x1 k-point grid. Additionally, the self-concistency cycle accuracy criterions were set to be 1 order of magnitude looser (e.g. `1E-4` instead of `1E-5`) to speed up calculations.

`boss.in` file The `boss.in` file contains all the keywords that are required or optional for a BOSS calculation. These keywords can be divided into three main sections: those that relate to the optimization, post-processing and other miscellaneous keywords. The latter set of keywords relate to aspects such as the parallelization on High Performance Clusters.

The optimization keywords can be viewed as the main set and contain the name of the user function (for example `userfn.py`), the bounds of the model and how many initial and/or iterative data points there should be. It also specifies the kernel, or covariance function, that should be used for optimization of the model. For all BOSS calculations performed the basic 'rbf' kernel was used with 200 initial and at least 50 iterative data points. If sampling was performed with a single atom the boundaries were set to the desired x, y and z values of a box located just above the surface. For diatomic molecules, where a rotational component should also be

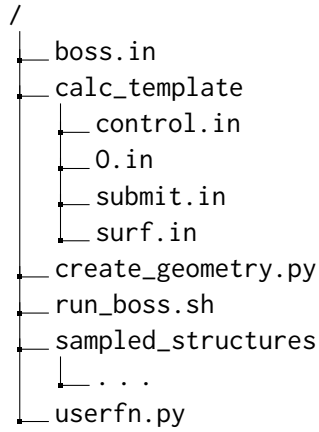

Figure 14: Structure of the directory and files when starting a calculation using BOSS.

incorporated, x, y and z values of the box were constrained around the found minimum and rotational boundaries for α, β, ɣ were added.

The post-processing keywords on the other hand dictate what BOSS should do once the optimization has finished and post-processing of the results is desired. This can include the determination of the local minima by selecting a percentage of the lowest acquisitions using ṕp_local_minima; alternatively a slice (2D map) can be made using the ṕp_model_slicekeyword in combination with the two variables that function as the x-axis and y-axis and how many data points each edge should have.

`userfn.py` script The user function has as its main function the return of data based on inputs received from the BOSS algorithm. The BOSS program provides an array with input data with the same structure as was defined in `boss.in` to the user function. It is then the job of the user function to take this array and provide the energy data for this point. How this is done is entirely up to the user, and for the performed work a FHI-AIMS `geometry.in` is created by combining a surface slab with the desired atom/molecule using the provided coordinates. This is then moved to its own created directory in a śampled_structuresdirectory where the FHI-AIMS calculation is performed, the resulting file structure for a BOSS calculation can be seen in figure 14. After the calculation, the resulting energy is read from the output and provided to BOSS in order to obtain the next desired data point.

A.3. Nudged Elastic Band

Nudged Elastic Band calculations were used to find the minimum energy pathways (MEPs) for the dissociation of species on the coated surface. For these NEB calculations the implementation of the Atomic Simulation Environment (ASE)[52] was used for the determination of future data points [50] whilst FHI-AIMS was used for the single point (DFT) calculations. To perform the NEB calculation with ASE and FHI-AIMS a python script to guide ASE on what to do is required in addition to a intial and final structure. THe initial and final structure could be obtained by performing a geometry optimization of structures that are close to the desired or expected

states. The python script was then used to take the initial and final state and perform a linear interpolation between them with the desired amount of images. These images are the structures that will be changed during the NEB to investigate the Minimum Energy Path between the initial and final state.

After the script performed the interpolation, it prints a control file for FHI-AIMS with the keywords described in appendix A.1 to use for the single point calculations. Afterwards the optimization algortihm is set and this is used by the optimizer can be set with a variety of choices, with the Fast Intertial Reference Engine (FIRE)[59, 60] algorithm being chosen for the NEB calculations performed in this work. The optimizer determines from the existing geometries and calculated single point energy what 'direction' to take the structures to obtain a MEP, the movement of the atoms is here constrained by the NEB method that placed an 'elastic band' between the images to not let the images cluster [60]. When the optimizer is set the python script sets the calculator that calculates the energies (FHI-AIMS in this work) and gives ASE the start command to perform the NEB until a certain criteria is met, which was a residual forces maximum of 0.1 eV/Å (`Fmax = 0.01`). Then, when the NEB has finished it is possible to analyze the energies of the images and perform a Climbing Image (CI) run.

The Climbing Image[51] run is performed to obtain a more accurrate structure and energy of the transitions state (TS). To perform this an initial and final structure are taken around the highest energy point in the original NEB. With these structures a procedure similar to the original NEB was performed, but instead of using a normal NEB the keywork for a climbing image run (`climb=True`) is added. During this run the images are not changed to obtain only the MEP, but also to obtain the saddle point of the Potential Energy Surface (PES) which is the transition state. These NEB calculations were also performed using a slightly tighter convergence criterium with a maximum residual forces parameter of 0.05 eVÅ. The transition state and minima before and after the TS could then be calculated using the *tight* basis set to obtain more accurate energies for these structures to determine the activitation energy and energy difference of the transition.

B. Density of States

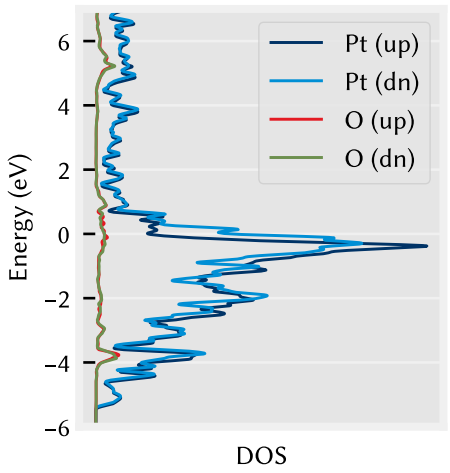

Figure 15: Species projected and spin polarized DOS of the top layer of the Pt coated surface and the oxygen molecule before dissociation.

C. Adsorption sites

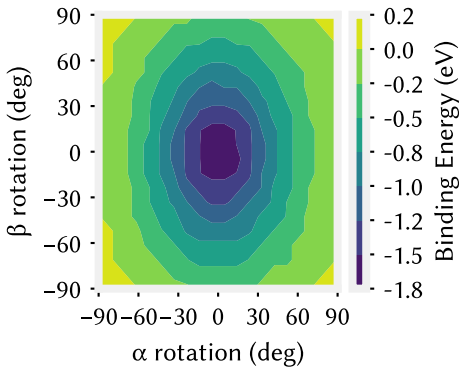

Figure 16: Species projected and spin polarized DOS of the top layer of the Pt coated surface and the oxygen molecule before dissociation.

D. Poster Presentations

Poster presentations of this thesis were given at the following conferences:

- NWO CHAINS, 21–22 September 2022, NH Koningshof Veldhoven
- The first e-CHEMS & S4S Symposium, 21 October 2022, Utrecht
- nanoGe INTERECT22, 21–22 November 2022, Valencia, Spain

The poster is reproduced below.

Utrecht University

Debye Institute for Nanomaterials Science

MCC Materials Chemistry and Catalysis

Understanding the composition of CuAu/Pt Nanoalloy Catalysts with DFT and Machine Learning

Robin van der Kruit (5895014), Nong Artrith

Materials Chemistry and Catalysis (MCC), Debye Institute of Nanomaterials, Utrecht University, the Netherlands

Contact: r.vanderkruit@students.uu.nl and n.artrith@uu.nl

Abstract

Multimetallic nanoparticles can leverage the synergistic effects between the component metals for improved characteristics with a potential reduction in the scarce material usage. Building on earlier theoretical and experimental investigations into bimetallic CuAu nanoparticles, the addition of **a Pt shell is expected to improve the activity, potentially making the trimetallic system an alternative for pure Pt.**

The CuAu/Pt core/shell particles were investigated as slab models using DFT calculations. The Pt adsorption sites were identified on an Au-terminated (100) CuAu surface using Bayesian Optimization Structure Search (BOSS) and a monolayer of Pt was adsorbed on the surface and the adsorption energy was investigated. This was followed by Nudged Elastic Band (NEB) analysis of the O_2 dissociation on the Pt-coated surface.

Computational Methods: Combined DFT & Machine Learning (ML)

DFT: FHI-AIMS code[1]

Density Functional Theory (DFT) calculations were performed using all-electron electronic structure theory with numeric atom-centered orbitals as implemented in FHI-aims.

The PBE density functional with the van-der-Waals correction by Tkatchenko and Scheffler was used. All energies were converged with a "tight" FHI-aims basis set, using a 12×12×1 k-point mesh for the integration of the Brillouin zone, the Atomic Zora scalar relativistic correction and no spin polarization.

ML: BOSS (Bayesian Optimization Structure Search)[2]

Pt adsorption sites were sampled in a specified region (x, y, z bounds), using Bayesian Optimization to find the global minimum.

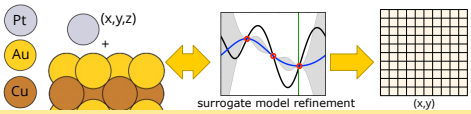

ML: NEB (Nudged Elastic Band)

Interpolation between initial and final state with DFT calculations for each point. After energy calculation, images are optimized to identify the minimum energy path (MEP) and transition state (TS).

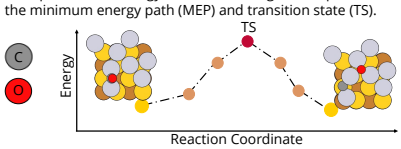

Summary & Outlook

It was found that Pt adsorbs on the hollow sites of the CuAu(100) surface and forms a monolayer instead of clusters. On one of the resulting surfaces the adsorption of CO, O_2, C and O was investigated and the MEP for the dissociation of O_2 was determined using NEB.

Further understanding can be gained by investigating the Density of States (DOS). Furthermore, the investigation can be expanded to the adsorption and dissociation of CO and H_2 on the surface. Additionally, expanding this study to other facets of the CuAu alloy and including an analysis of the surface strain can provide valuable insights for the interpretation of experimental results.

Results: Pt Adsorption

Pt addition based on BOSS results with 3 methods and two-step geometry optimization:

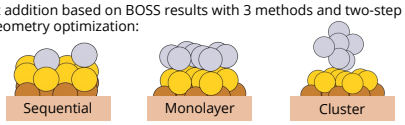

Adsorption Energy

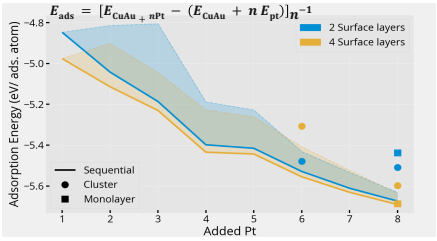

Based on the figure, it is favourable for the Pt to fill the surface (1:1 Au:Pt). After geometry optimisation of 4 surface layers, the Pt is located around the hollow sites.

Results: O Atom Adsorption Sites

On one of the Pt coated surfaces, BOSS was used to determine the preferred adsorption sites of atomic Oxygen. Comparing the Pt-coated surface and O-sampled surface allows for determination of the binding sites.

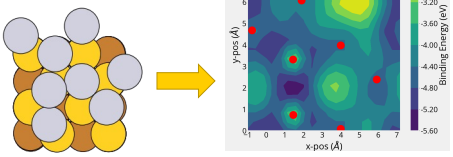

Results: O_2 Dissociation

From the initial state with O_2 to the final state with 2 atomic O the MEP could be investigated using NEB. The NEB was performed with 5 images and the light basis set.

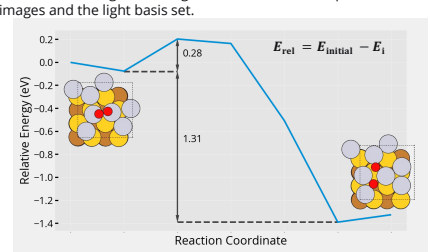

From the NEB the O_2 dissociation has an activation energy of 0.28 eV and total energy change of 1.31 eV, which is in agreement with existing literature values of ~0.3 eV [3].

Acknowledgements

Computer resources from NWO SURFsara and discussions with Dr. de Groot, Dr. van der Hoeven and the MCC group are gratefully acknowledged.

References

[1] V. Blum, R. Gehrke, F. Hanke, P. Havu, V. Havu, X. Ren, K. Reuter, M. Scheffler, *Computer Physics Communications* **2009**, *180*, 2175–2196.

[2] M. Todorović, M. U. Gutmann, J. Corander, P. Rinke, *Npj computational materials* **2019**, *5*, 35.

[3] P. Jennings, H. Aleksandrov, K. Neyman, *Nanoscale* **2014**, *2*, 1153-1165.